

MALAYSIAN JOURNAL OF MICROSCOPY

Journal homepage: https://malaysianjournalofmicroscopy.org

RESEARCH ARTICLE

FABRICATION OF UNIFORM POROUS LAMELLAR ZINC STRUCTURES BY DEALLOYING OF EUTECTIC BINARY ZINC-ALUMINIUM ALLOYS

Muhammad Afiq Irfan Mohd Shumiri¹, Abdillah Sani Mohd Najib^{1,2}, Nor Akmal Fadil^{1,2,*}

¹Materials Research and Consultancy Group, Faculty of Mechanical Engineering, Universiti Teknologi Malaysia, Johor Bahru, Malaysia.

²Department of Materials, Manufacturing and Industrial Engineering, Faculty of Mechanical Engineering, Universiti Teknologi Malaysia, Johor Bahru, Malaysia.

Abstract. Porous metallic zinc is a promising hostless electrode material for zinc-based energy storage applications due to excellent electrochemical behavior. Among various fabrication methods, dealloying stands out for its simplicity and efficiency. However, challenges such as uneven pore distribution and uncontrollable pore structures compromise the quality of porosity. In this study, highly uniform porous lamellar zinc structures were developed through chemical dealloying of the eutectic binary zinc-aluminium alloy system. The resultant lamellar configuration was finely tuned by adjusting the precursor alloy composition and bimetallic phase distribution. A homogenous zebra-like quasi-periodic lamellar pattern was achieved at eutectic composition of Zn₉₅Al₅ (wt%). This structure exhibited greater uniformity compared to the eutectoid-rich lamellar structure observed in the hypereutectic Zn₉₀Al₁₀ alloy. A large Zn lamellar thickness of 2919.7 ± 371.0 nm and interlamellar spacing of 1248.3 ± 203.6 nm were produced under low solidification rate by furnace cooling. Optimal dealloying parameters of 4 M NaOH at 50 °C were determined, providing ideal balance between the reaction rate and structural stability. The thick lamellae promoted high dealloying rate of 1.988 mg/cm²/h, resulting in high peak-to-valley roughness of 3698 nm. Selective dissolution of the less noble aluminium component left behind the alternating zinc-rich lamellar framework as examined by variable-pressure scanning electron microscopy (VPSEM), atomic force microscopy (AFM) and X-ray diffraction (XRD) spectroscopy. This structure endows abundant pores with consistent interlayer spacing.

Keywords: Lamellar structure, porous zinc, eutectic alloy, selective leaching, dealloying.

Article Info

Received 31 December 2024 Accepted 6 March 2025 Published 2 June 2025

*Corresponding author: norakmal@utm.my

Copyright Malaysian Journal of Microscopy (2025). All rights reserved.

ISSN: 1823-7010, eISSN: 2600-7444

1. INTRODUCTION

Porous metallic zinc holds particular promise as the hostless electrode material for zinc-based energy storage applications due to high electrochemical performance [1]. In contrast to conventional planar zinc, it suffers from low surface area, poor wettability, surface passivation and restricted ion transport pathways [2]. These limitations hinder the practical use of zinc electrode especially in zincion batteries, supercapacitors and fuel cells. Among various fabrication methods, chemical dealloying has emerged as the effective approach for producing porous zinc. In this process, the etchant reacts spontaneously with the precursor alloy under free corrosion conditions, selectively dissolving the less noble element and leaving behind the porous network of the more noble metal [3]. This technique provides additional advantage of tunable pore structures, allowing key parameters such as surface area, porosity and mechanical robustness to be optimized by adjusting dealloying conditions like temperature, etchant concentration, precursor composition and phase distribution [4]. However, the commonly adopted dealloying conditions remain limited and challenges such as coarsening effects, uneven pore distribution and uncontrollable ligament structures can compromise the quality of porosity. This highlights the need for more controlled fabrication of porous zinc structures. Achieving uniform porosity requires homogeneous phase in the parent alloy system [5]. Hence, Zn-Al alloy is the best candidate for this purpose due to poor miscibility which allows for homogenous structure with zebralike lamellar stripes at eutectic composition, making it promising precursor for porous Zn. The lamellar thickness can be finely tuned by adjusting the cooling rate during solidification process [6]. Binary Zn-Al alloys have partial solubility limit without forming intermetallic compounds and the crystalline microstructure retains its original grain orientation during dealloying [7]. The fine and even distribution of eutectic structure ensures that when the less noble component is selectively leached out, the resultant pores are highly distributed throughout the Zn matrix. The remaining noble metal forms lamellar ligament that generally mirrors the phase structure of precursor alloy. Indeed, the regularity of alternating lamellar structure leads to consistent pore and ligament distribution after dealloying.

This study focuses on the development of highly uniform porous zinc structures by tailoring the microstructure of Zn-Al alloys prior to dealloying. To examine the influence of alloy composition on lamellar uniformity, both hypereutectic and eutectic Zn-Al alloys were investigated. Lamellar thickness was controlled by adjusting the solidification rate using various cooling techniques, including water, air and furnace cooling. Solidification behavior plays important role in determining the final phase distribution, as it governs atomic diffusion during the transition from liquid to solid [8]. Following microstructural optimization, a systematic dealloying study was conducted to evaluate the effects of temperature and etchant concentration on pore formation and structural integrity. Morphological changes during dealloying were characterized using scanning electron microscopy (SEM), providing insight into the pore evolution mechanism. Aluminium was selectively dissolved due to its amphoteric nature, high reactivity and cost-effectiveness, making it an ideal sacrificial element for porous zinc synthesis [9]. Overall, this research aims to establish a controllable and scalable dealloying strategy for fabricating robust lamellar porous zinc frameworks with high structural uniformity. These findings offer valuable insights for the electrode design of next-generation zinc-based energy storage systems.

2. MATERIALS AND METHODS

2.1 Preparation of Zn-Al Precursor Alloy

Hypereutectic Zn₉₀Al₁₀ (wt.%) and eutectic Zn₉₅Al₅ master alloys were prepared using metallurgical induction melting technique. Heavy metal furnace (Nabertherm, T110/11) was used for melting with temperature set to 750 °C. High-purity Zn (99.6%) and Al (99.0%) were melted in ceramic crucible and the molten alloy was continuously stirred with graphite rod to ensure thorough mixing. The alloy was cast into ingots under controlled cooling conditions using water, air and furnace cooling methods. Once solidified, the ingots were extracted and the surface oxide layer was removed. The areas that solidified directly with the molds were removed because these chilled zones tend to have

significantly different microstructure. These peripheral regions interfere with the uniform lamellar pattern desired in the specimens. Subsequently, the remaining alloy was sectioned into sheets of 1 mm thickness with cuts made perpendicular to the lamellar structure. $Zn_{90}Al_{10}$ and $Zn_{95}Al_5$ alloy sheets were then mechanically polished with 0.05 μ m finishing and prepared for characterization. The weight of alloy sheets was measured and recorded.

2.2 Preparation of Porous Lamellar Zn

Porous lamellar Zn was fabricated using free corrosion method. Eutectic $Zn_{95}Al_5$ alloy sheets were chemically dealloyed in which the less noble Al constituent was selectively dissolved in strong alkaline etchant. By using concentrated sodium hydroxide (NaOH) as a leaching solution, the reaction $2Al + 6H_2O + 2NaOH \rightarrow 2NaAl(OH)_4 + 3H_2$ occurred when the samples were placed inside corrosive NaOH medium. The samples were immersed in 2 M, 3 M, 4 M and 5 M NaOH at temperature of 25 °C, 40 °C, 50 °C and 60 °C, respectively, for 4 h to evaluate the effect of etchant concentration and dealloying temperature on the dealloying rate and the resultant porous morphology. Thereupon, the asdealloyed porous Zn was rinsed several times in ethanol and cleaned using continuous ultrasonication in distilled water for 10 minutes to stop the corrosion process. The samples were dried for 2 h at 100 °C in the oven with argon gas to remove any moisture. Lastly, the weight of samples was measured and recorded.

2.3 Materials Characterization

Zn₉₀Al₁₀ and Zn₉₅Al₅ alloy sheets were first prepared through conventional grinding and mechanical polishing to obtain smooth surfaces for analysis. The metallographic microstructure was then examined using laboratory optical microscope (Nikon, Eclipse LV150) to observe the structural features. Detailed electron micrographic analysis was performed using variable-pressure scanning electron microscope (VPSEM) (Zeiss, Supra VP35) which was equipped with on-system energy-dispersive X-ray spectroscopy (EDS) for elemental analysis. The Zn lamellar thickness (λ_t) and interlamellar spacing (λ_s) distribution were determined by manually measuring the width of 200 randomly selected lamellae, with measurements taken perpendicular to the lamellar direction. Additionally, X-ray diffraction (XRD) (Rigaku, SmartLab2018) measurements were carried out using D/max2500pc diffractometer with Cu Kα radiation for phase identification and crystallographic analysis. Diffraction data were recorded over 2θ range of 20° to 80° with scanning speed of 2° per minute and step size of 0.02°. 3D surface morphology of the as-dealloyed porous lamellar Zn was analyzed using atomic force microscope (AFM) (Bruker, Multimode 8) operating in tapping mode, which allows for high resolution scanning. The scan sizes of 10 μm was employed in both X and Y directions, with Z-axis range set to 15 μm.

3. RESULTS AND DISCUSSION

3.1 Materials Characterization of Hypereutectic Zn₉₀Al₁₀ and Eutectic Zn₉₅Al₅ Alloy

The binary Zn-Al alloy system has distinctive microstructures depending on the composition due to limited miscibility of the two components. In hypereutectic $Zn_{90}Al_{10}$ alloy, a non-uniform lamellar structure is produced due to the formation of primary ZnAl (γ) phase which solidifies first at higher temperature before the eutectic reaction occurs. The solidification process is dominated by the characteristics of primary ZnAl (γ) phase which disrupt the consistency of lamellar pattern. This initial phase develops large zone that are interspersed within the structure. As temperature drops to 381 °C, the remaining liquid undergoes eutectic reaction and transforms into two solid phases, Zn (β) and ZnAl (γ). However, by this stage, the composition of remaining liquid has changed that causes irregular eutectic solidification behavior. The solid phases tend to nucleate and grow in localized regions rather than uniformly distributed throughout the structure. Subsequently, when the temperature reaches 275 °C, ZnAl (γ) phase undergoes eutectoid reaction and transforms into Al (α) and Zn (β). This

sequential solidification process results in inhomogeneous lamellar arrangement due to the formation of distinct phases at different stages. These phases are randomly distributed in extensive zones as well as smaller colonies (Figure 1a-b). The large dark regions are characterized by the presence of both Zn (β) and Al (α) phases in a complex eutectoid lamellar structure (Figure 1c). This result was confirmed by SEM image (Figure 1d) and the corresponding EDS elemental mapping of Zn (Figure 1e) and Al (Figure 1f).

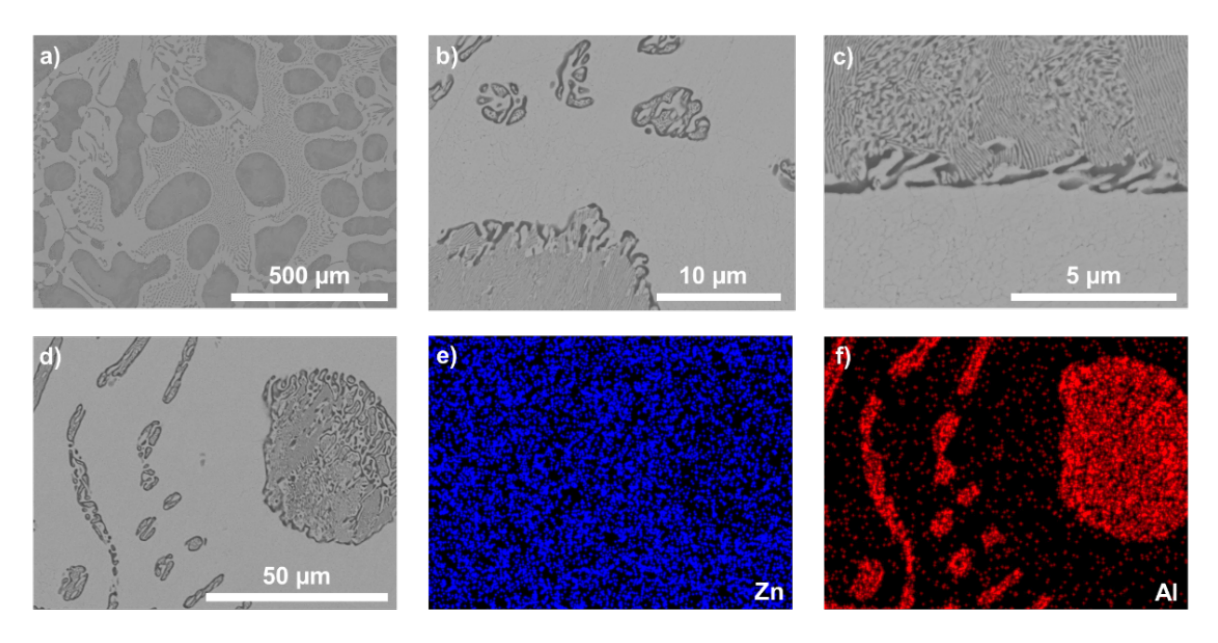


Figure 1: SEM micrographs of hypereutectic Zn₉₀Al₁₀ alloy (a) Uneven phase distribution of Zn and Al components across the alloy matrix, (b) Eutectoid structure in extensive zones and small colonies, (c) Eutectoid structure composed of lamellar arrangement and complex random pattern, (d) SEM image with corresponding EDS mapping of (e) Zn and (f) Al

For Zn₉₅Al₅, both Zn and Al constituents crystallize concurrently from the molten solution. Based on the phase diagram in Figure 2, a single liquid phase transforms into two solid phases, Zn (8) and ZnAl (γ), simultaneously during eutectic reaction at 381 °C. Then, the three-phase eutectoid reaction occurs at 275 °C that transforms a single solid phase of ZnAl (γ) into two different solid phases, Al (α) and Zn (β) . The eutectic reaction produces a well-ordered alternating lamellar structure composed of predominantly Zn (β) phase and ZnAl (γ) phase. Due to the coexistence of these two solid phases, the lamellae grow side by side in parallel array along with the longitudinal direction which is parallel to the heat flow during solidification. The lateral diffusion of excess Zn and Al towards the solid-liquid interface is equilibrium with the formation of Zn/Al interfacial areas. The proximity of the two phases minimizes diffusion distances, making it energetically favorable to grow in tandem. Therefore, Zn (β) phase and ZnAl (γ) phase produce very unique alternating lamellar morphology as shown in Figure 3ab. The bright regions represent Zn (β) phase while the dark regions correspond to Al (α) phases. This result was confirmed by elemental mappings obtained through EDS in Figure 3c-e. Each lamella remains continuous within individual grains but is interrupted by grain boundaries that delineate regions where the orientation of lamella varies (Figure 3f). Within each grain, the lamellae maintain a consistent spacing and orientation, resulting in a well-defined and uniform microstructure. Grain boundaries arise at the interfaces between grains with differing crystallographic orientations. These boundaries introduce slight misalignments at the junctions while preserving the integrity of lamellar configuration.

Utilizing the binary phase system simplifies the subsequent dealloying processes which makes this approach efficient to fabricate porous materials. In this context, the eutectic $Zn_{95}Al_5$ is particularly ideal as a parent alloy for dealloying applications. This alloy was characterized by its regular lamellar pattern which demonstrates superior potential to achieve consistent porosity compared to the hypereutectic $Zn_{90}Al_{10}$ alloy. The uniformity of lamellar structure is critical to attain high quality

porosity, as it promotes more predictable dissolution dynamics during the dealloying process. Both Al (α) and Zn (β) phases coexist and remain stable at room temperature according to Zn-Al phase diagram (Figure 2).

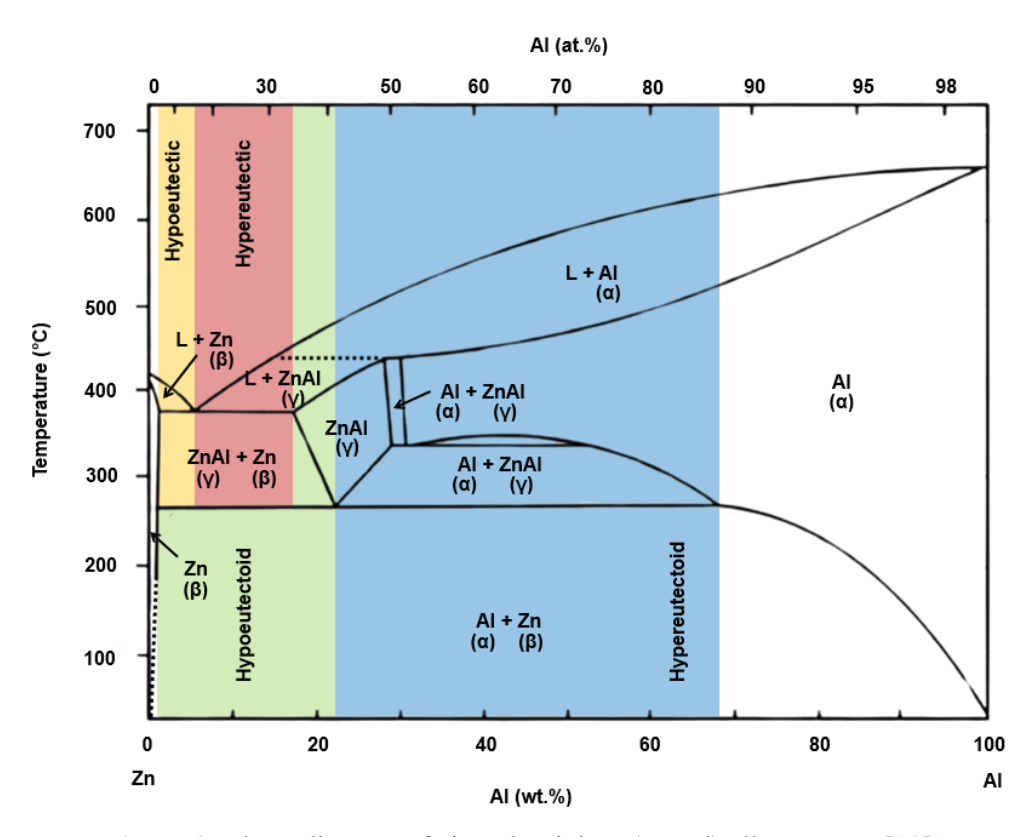


Figure 2: Phase diagram of zinc-aluminium (Zn-Al) alloy system [10]

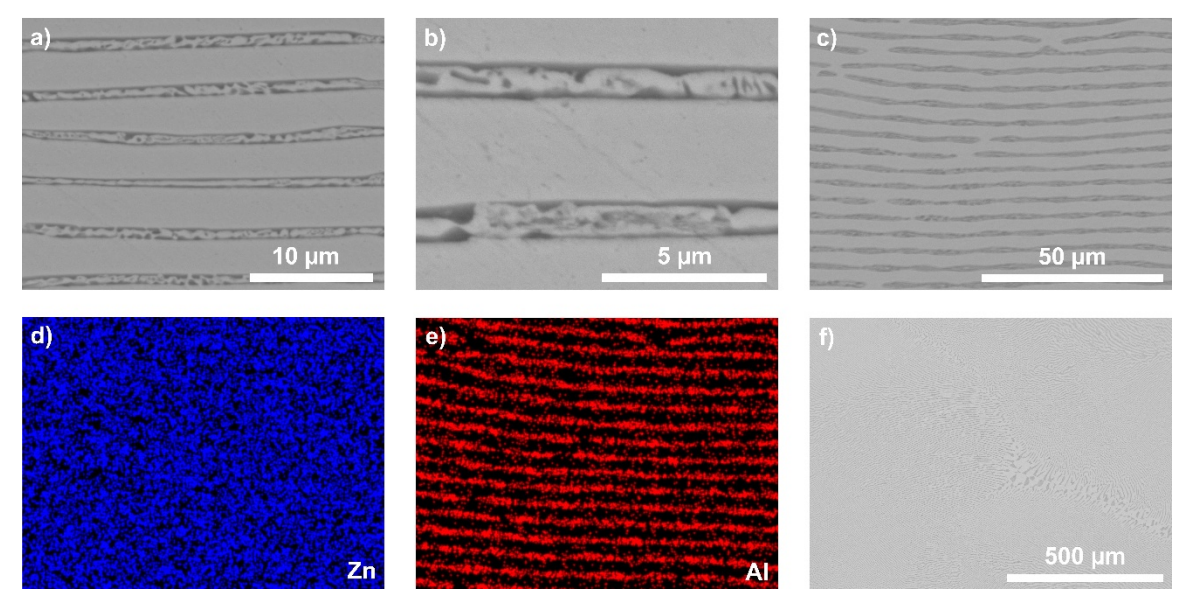


Figure 3: SEM micrographs of eutectic Zn₉₅Al₅ alloy. (a) Eutectic structure composed of highly uniform alternating lamellae of Zn and Al components. (b) Complex eutectoid structure composed of randomly distributed Zn and Al components that transform from the original eutectic morphology. (c) SEM image with corresponding EDS mapping of (d) Zn and (e) Al. (f) Grain boundary region that shows the distinct boundaries separating adjacent grains

However, the final phase distribution is significantly affected by the solidification process. The growth of solid phases relies on atoms diffusion from liquid into solid. When the cooling rate increases, both λ_t and λ_s decrease because rapid solidification limits the time available for atomic diffusion. Under faster cooling conditions, the difference between actual liquid temperature and eutectic temperature becomes more pronounced due to fast heat extraction. This higher degree of undercooling promotes the formation of more nucleation sites [11]. Admittedly, Liu et al. [12] agreed that higher cooling rate could reduce the grain size. Consequently, the solid phases grow closer together. Water-cooled induces the most rapid cooling rate that produces the finest interspersed lamellar with λ_t of only 307.0 ± 84.3 nm and λ_s of 108.8 ± 20.8 nm (Figure 4a-c). As expected, the Al component does not have sufficient time to diffuse uniformly throughout the structure, resulting in the precipitation of Al (α) phase in localized areas as the structure rapidly solidifies. Additionally, air-cooled lamellae are slightly thicker with λ_t at 745.8 ± 150.2 nm and λ_s at 250.1 ± 45.4 nm (Figure 4d-f). In contrast, under furnace-cooled condition, λ_t reaches 2919.7 ± 371.0 nm and λ_s is 1248.3 ± 203.6 nm (Figure 4g-i). This relatively slow cooling allows more time for atomic diffusion and results in bigger lamellae.

Precursor alloy Water-cooled Air-cooled Furnace-cooled a) d) g) 10 μm 10 µm b) e) h) $\lambda_{i} = 745.8 \pm 150.2 \text{ nm}$ $\lambda_t = 307.0 \pm 84.3 \text{ nm}$ $= 2919.7 \pm 371.0 \text{ nm}$ 60 60 140 20 20 Count 40 Count 20 20 1000 300 400 400 600 800 3000 Zn lamellar thickness, λ_t (nm) Zn lamellar thickness, λ, (nm) Zn lamellar thickness, λ, (nm) f) ₆₀ C) $= 108.8 \pm 20.8 \text{ nm}$ = 250.1 ± 45.4 nm = 1248.3 ± 203.6 nm 80 80 th 40 20 60 Gorif 5 60 40 20 20 100 120 140 160 180 200 150 200 250 1200 1600 2000 Zn interlamellar spacing, λ_s (nm) Zn interlamellar spacing, λ_s (nm) Zn interlamellar spacing, λ_s (nm)

Figure 4: SEM micrographs of eutectic Zn₉₅Al₅ alloy solidified under different cooling conditions along with the corresponding distributions of Zn lamellar thickness and interlamellar spacing. (a-c) Water-, (d-f) air- and (g-i) furnace-cooled condition

3.2 Materials Characterization of Porous Lamellar Zn Alloy

Porous lamellar Zn structure was prepared using free corrosion method through controlled chemical dealloying in NaOH solution. Table 1 shows dealloying rate and weight loss percentage after 4 h dealloying in various etchant concentrations and temperatures for precursor $Zn_{95}Al_5$ alloy. Based on Table 1, up to ~22% weight reduction occurs after dealloying which is consistent with the selective corrosion of Al (α) phase. This occurs due to the amphoteric nature of Al which very well dissolves in alkaline electrolyte [13]. In this case, Al (α) component reacts with concentrated NaOH solution to form complex sodium aluminate ions and hydrogen gas ($2Al + 6H_2O + 2NaOH \rightarrow 2NaAl(OH)_4 + 3H_2$). The dissolution of Al (α) is facilitated by hydroxide ions (OH) that break down the protective oxide layer

to allow for further removal $(Al_2O_3 + 2OH^- + 3H_2O \rightarrow 2Al(OH)_4^-)$. At the same time, H_2 bubbles were immediately released during this process that visually confirms the ongoing chemical reaction. In electrochemical terms, Al is more anodic, having more negative standard electrode potential $(Al^{3+}/Al = -1.66 \text{ V})$ compared to $Zn (Zn^{2+}/Zn = -0.76 \text{ V})$ which makes Al more likely to lose electrons and prone to oxidation [14]. This difference in electrode potentials establishes galvanic effect. Indeed, according to Pourbaix analysis, Al is thermodynamically unstable in high pH environment and susceptible to corrosion [15]. Therefore, Al (α) was considered as less noble element compared to $Zn (\beta)$ in the binary Zn-Al alloy system.

Table 1: Dealloying rate and weight loss percentage after 4 h dealloying in various etchant concentrations and temperatures for precursor Zn₉₅Al₅ alloy

Precursor alloy	Etchant conc. (M)	Dealloying temp. (°C)	Weight (g)		Wai ab4	Deallaring vote
			Before dealloy	After dealloy	Weight loss (%)	Dealloying rate (mg/cm²/h)
Water-cooled	2	25	0.737	0.702	4.75	0.438
	3	40	0.712	0.665	6.60	0.587
	4	50	0.785	0.727	7.39	0.725
	5	60	0.752	0.663	11.84	1.113
Air-cooled	2	25	0.757	0.718	5.15	0.488
	3	40	0.802	0.745	7.11	0.713
	4	50	0.770	0.698	9.35	0.900
	5	60	0.713	0.604	15.29	1.363
Furnace-cooled	2	25	0.784	0.718	8.42	0.825
	3	40	0.741	0.632	14.71	1.363
	4	50	0.812	0.653	19.58	1.988
	5	60	0.824	0.639	22.45	2.313

The removal of Al (α) phase became apparent in 2 M NaOH at room temperature (25 °C) after 4 h of dealloying (Figure 5a-c). The three-dimensional porous lamellar structure was produced that periodically interleaved with layers of Zn (β) lamellae. However, the noble Zn component slightly dissolves in localized areas, even as selective removal of Al occurs simultaneously. This dissolution is due to the tightly interlocked and closely intermixed Zn (β) and Al (α) phases, which constrain each other in the eutectoid arrangement. As dealloying process occurs, high mobility of Zn atoms rearranges and occupy the voids left by the dissolved Al atoms. Initially, according to atomistic hard sphere model, Al atoms are more susceptible to leach out at low coordination sites such as step edges which dissolve more quickly than atoms at higher coordination sites [16]. Consequently, Al (α) phase is stripped away layer by layer. Instead of forming a stable structure, Zn atoms migrate along these step edges, causing an expansion of porosity as additional layers are removed. This leads to the breakdown of original eutectoid architecture.

In order to further optimize dealloying process, key parameters such as temperature and etchant concentration were fine-tuned. Increasing the temperature from 25 °C to 50 °C accelerates the etching process as the ions gain additional energy which improve their mobility to allow for more efficient interaction at the alloy interface. Likewise, the increase in NaOH concentration from 2 M to 4 M also accelerates the dealloying rate due to higher availability of OH $^-$. The abundance of OH $^-$ enhances reaction kinetics and directly increases Al (α) corrosion rate. This rapid dissolution leads to more efficient dealloying process which is crucial to achieve the desired porous structure. However, it is critical to maintain a balance between surface diffusion and dissolution to form a well-structured lamellar porous network. Despite rapid removal of Al, the more stable Zn component remains largely intact with minimal atomic rearrangement. Zn (β) component retains the original lamellar configuration that reflects the initial morphology of precursor eutectic alloy. While some localized surface diffusion of Zn (β) occurs, it does not significantly disrupt the overall structure. The general lamellar framework remains preserved and resembled after dealloying even at higher NaOH concentrations and temperature (Figure 5d-i).

However, under an aggressive corrosive medium of 5 M NaOH at 60 °C, the samples experience significant degradation that results in the formation of crack (Figure 5j-l). Substantial gaps emerge between the remaining lamellae that grow in several microns wide. Once cracks initiate, they propagate along the interlamellar region. Although cracks may become arrested at certain interfaces, the overall degradation continues as they spread through the structure. This dealloying-induced cracking is prevalent in thin lamellar structure of eutectic Zn₉₅Al₅ alloy under rapid solidification conditions by water- and air-cooled. The thin lamellae contain higher density of defects which act as initiation sites for cracking [17]. During the dealloying process, mechanical stress develops from internal factors primarily due to the resultant structural changes. These stresses tend to concentrate around defects which make the structure more prone to cracking. As the less noble Al (α) component was removed, volume reduction occurred in certain regions while the remaining component retained the original dimensions. This uneven removal creates internal stresses as the structure attempts to accommodate the resulting volume changes, leading to mechanical strain [18].

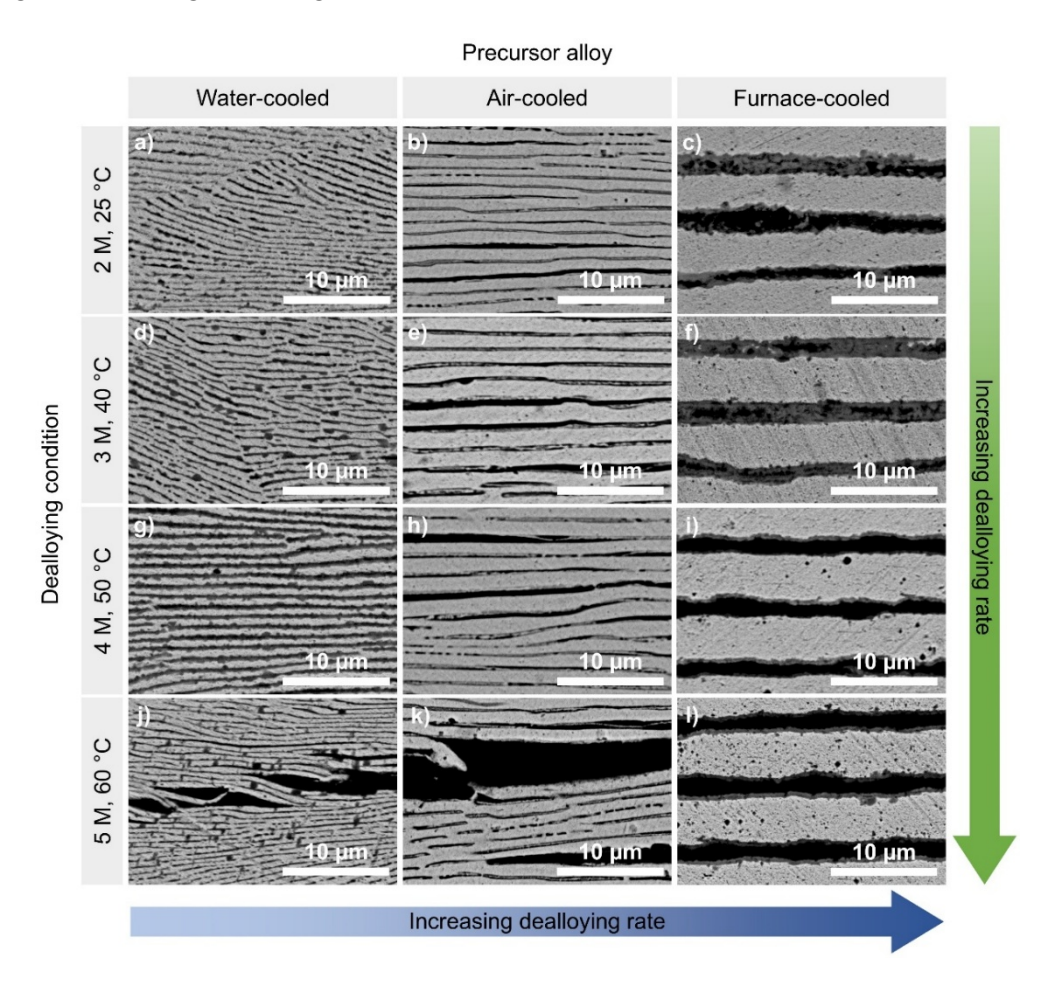


Figure 5: SEM micrographs of precursor Zn₉₅Al₅ alloy after 4 h dealloying under different etchant concentrations and temperatures with correlation to dealloying rate. (a-c) 2 M NaOH at 25 °C, (d-f) 3 M NaOH at 40 °C, (g-i) 4 M NaOH at 50 °C and (j-l) 5 M NaOH at 60 °C

For this reason, dealloying in 4 M NaOH at 50 °C was identified as the optimal condition, as it achieved high dealloying rate while simultaneously preserving the structural integrity. This parameter is ideal for developing a well-defined porous lamellar structure, as it balances efficient dissolution with the retention of desired framework. The fine lamellar pattern of water-cooled precursor limits the selective dissolution of Al. Rapid nucleation during solidification produces fine grains with closely spaced lamellae, which help suppress localized corrosion and reduce galvanic coupling between Zn and Al phase. A similar effect is observed in the air-cooled precursor, where moderately fine lamellae also minimize the corrosion effect of Al. In contrast, the thick lamellae of furnace-cooled precursor show

more pronounced Al dissolution, resulting in the formation of large lamellar pores within the Zn matrix. Figure 6 presents XRD analysis of the dealloyed Zn₉₅Al₅ sheets. The face-centered cubic Al diffraction peak have diminished because the less noble Al component is preferentially leached out. Meanwhile, the dominant peaks of hexagonal close-packed Zn phase remain. The Zn peaks observed at 36.3°, 38.9°, 43.2°, 54.3°, 70.1° and 70.6° correspond to the (002), (100), (101), (102), (103) and (110) planes of Zn, respectively. Additionally, as shown in Figure 7, SEM images with corresponding EDS mapping revealed that Al constituents are minimally present and randomly distributed, in contrast to the well-structured lamellar pattern observed prior to dealloying. Dealloyed region also shows minimal presence of oxide components, indicating that no significant oxidation occurs after dealloying process.

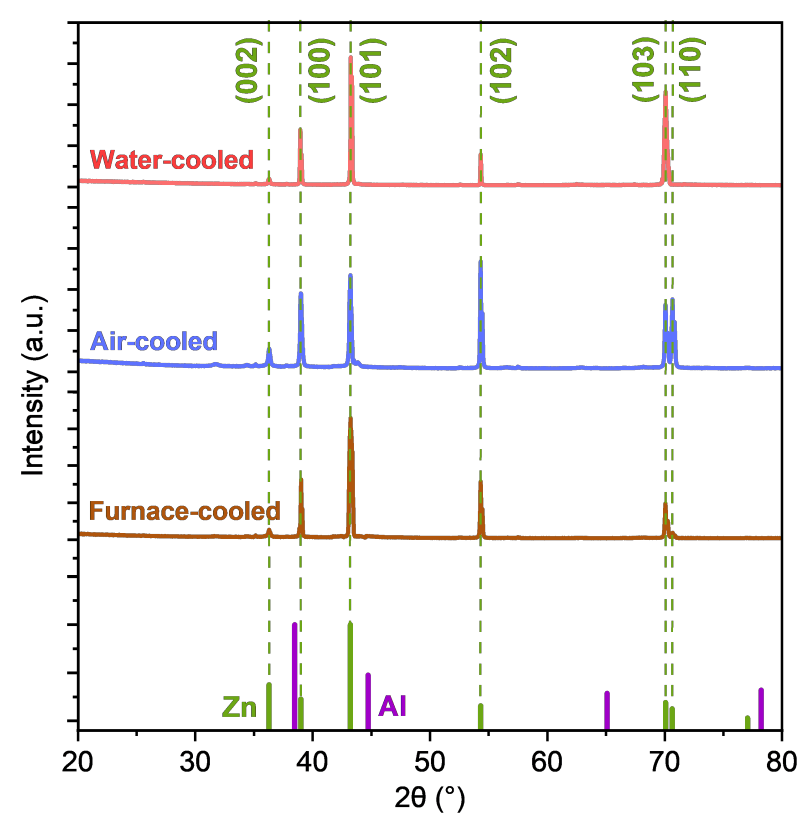


Figure 6: XRD patterns of water-, air- and furnace-cooled eutectic Zn₉₅Al₅ alloy after 4 h dealloying in 4 M NaOH at 50°C. The line patterns show reference cards 04-0831 and 04-0787 for Zn and Al according to JCPDS, respectively

AFM imaging was conducted in tapping mode to analyses the surface morphology of porous lamellar structure. The evolution of porosity is influenced by λ_t . Smaller λ_t experiences relatively limited dealloying depth compared to their thicker counterparts. Selective dissolution primarily occurs near the surface, gradually reaching saturation point where limited bulk diffusion pathways constrain further dealloying [19]. In contrast, bigger λ_t offers more continuous percolation paths, allowing deeper penetration and sustained diffusion of active species throughout the surface. This enables for more extensive leaching of the less noble component from the alloy matrix. Therefore, larger lamellae experience more comprehensive dealloying depth. Based on Figure 8, after 4 h dealloying in 4 M NaOH at 50°C, furnace-cooled precursor shows higher peak-to-valley roughness, R_t (3698 nm) compared to the air- (595.1 nm) and water-cooled precursor (432.2 nm). This trend aligns with the observation that as λ_t increases, dealloying rate also increase, further highlighting the role of lamellar spacing in governing dealloying dynamics.

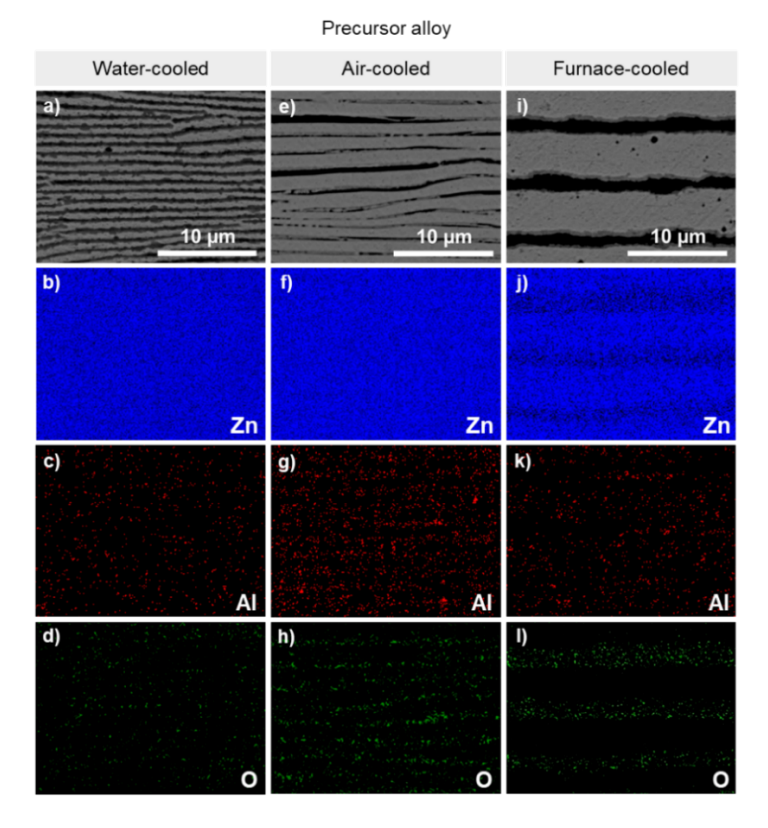


Figure 7: SEM images with corresponding EDS mapping for (a-d) water-, (e-h) air- and (i-l) furnace-cooled Zn₉₅Al₅ alloy after 4 h dealloying in 4 M NaOH at 50°C

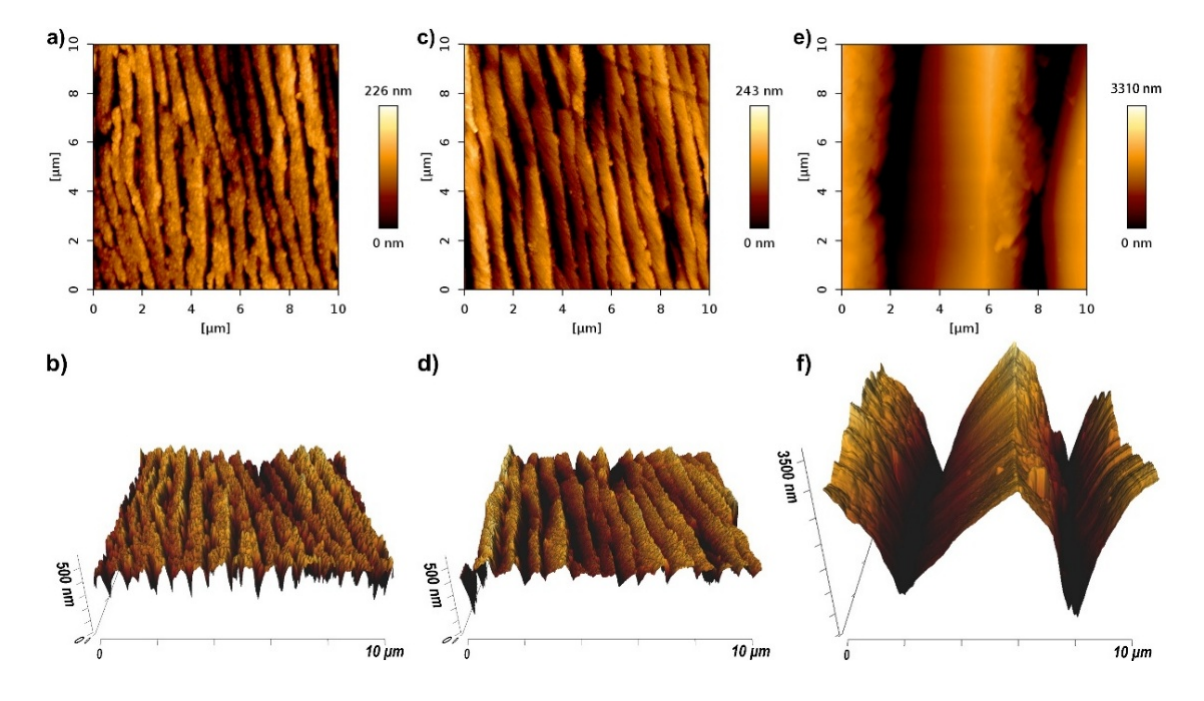


Figure 8: AFM images illustrating uniform distribution of lamellar structures with the corresponding 3D topographic showing the surface elevation profile after 4 h dealloying in 4 M NaOH at 50 °C for (a-b) water-, (c-d) air- and (e-f) furnace-cooled precursors

4. CONCLUSIONS

In conclusion, chemical etching of binary Zn-Al alloy system was successfully conducted to develop highly uniform porous lamellar Zn. The composition of Zn₉₅Al₅ alloy produced uniform lamellar structure due to eutectic reaction that occur during solidification which transform liquid phase into two different solid phases simultaneously. By adjusting the solidification process during casting, larger λ_t was produced under slow solidification rate with furnace-cooled condition due to lower nucleation rate and lead to the formation of bigger nuclei that grow into thicker lamellae. Furthermore, dealloying process was optimized by adjusting the etchant concentration and temperature. Optimal dealloying parameter was determined to be 4 M NaOH at 50 °C, providing ideal balance between the reaction rate and structural stability. The furnace-cooled precursor, with large lamellar thickness of 2919.7 \pm 371.0 nm and interlamellar spacing of 1248.3 \pm 203.6 nm, achieved high dealloying rate of 1.988 mg/cm²/h. This resulted in high peak-to-valley roughness of 3698 nm, contributing to increase active surface area and enhance electrochemical activity. These features make the material a promising hostless electrode for zinc-based energy storage applications.

Acknowledgements

This work was financially supported by the Universiti Teknologi Malaysia under the grant scheme of UTM Fundamental Research (Q.J130000.3824.23H15). We thank the Materials Research and Consultancy Group, Faculty of Mechanical Engineering, Universiti Teknologi Malaysia for the research support towards this publication.

Author Contributions

All authors contributed toward data analysis, drafting and critically revising the paper and agree to be accountable for all aspects of the work.

Disclosure of Conflict of Interest

The authors have no disclosures to declare.

Compliance with Ethical Standards

The work is compliant with ethical standards.

References

- [1] Mohd Shumiri, M. A. I., Mohd Najib, A. S. & Fadil, N. A. (2025). Current status and advances in zinc anodes for rechargeable aqueous zinc-air batteries. *Science and Technology of Advanced Materials*, 26(1), 2448418.
- [2] Wang, W., Huang, G., Wang, Y., Cao, Z., Cavallo, L., Hedhili, M. N. & Alshareef, H.N. (2022). Organic acid etching strategy for dendrite suppression in aqueous zinc-ion batteries. *Advanced Energy Materials*, 12(6), 2102797.
- [3] Jian, Q., Guo, Z., Zhang, L., Wu, M. & Zhao, T. (2021). A hierarchical porous tin host for dendrite-free, highly reversible zinc anodes. *Chemical Engineering Journal*, 425, 130643.

- [4] Mohd Shumiri, M. A. I., Mohd Najib, A. S., Putra, A. E. E. & Fadil, N.A. (2025). Electrochemical and chemical dealloying of nanoporous anode materials for energy storage applications. *Science and Technology of Advanced Materials*, 26(1), 2451017.
- [5] Chen, X., Karasz, E., Badwe, N. & Sieradzki, K. (2021). Dynamic fracture and dealloying induced stress-corrosion cracking. *Corrosion Science*, 187, 109503.
- [6] Wang, S. B., Ran, Q., Yao, R. Q., Shi, H., Wen, Z., Zhao, M., Lang, X. Y. & Jiang, Q. (2020). Lamella-nanostructured eutectic zinc-aluminum alloys as reversible and dendrite-free anodes for aqueous rechargeable batteries. *Nature Communications*, 11(1), 1634-1643.
- [7] Sun, J., Zheng, X., Li, K., Ma, G., Dai, T., Ban, B., Yuan, Y., Wang, M., Chuai, M., Xu, Y., Liu, Z., Jiang, T., Zhu, Z., Chen, J., Hu, H. & Chen, W. (2023). Scalable production of hydrogen evolution corrosion resistant Zn-Al alloy anode for electrolytic MnO2/Zn batteries. *Energy Storage Materials*, 54, 570-578.
- [8] Wang, X., Zhang, Z., Ji, H., Xu, J., Huang, X. & Ma, Y. (2012). Dealloying of single-phase Al2Au to nanoporous gold ribbon/film with tunable morphology in inorganic and organic acidic media. *Applied Surface Science*, 258(22), 9073-9079.
- [9] Meng, H., Ran, Q., Dai, T. Y., Jia, J. H., Liu, J., Shi, H., Han, G. F., Wang, T. H., Wen, Z., Lang, X. Y. & Jiang, Q. (2024). Lamellar nanoporous metal/intermetallic compound heterostructure regulating dendrite-free zinc electrodeposition for wide-temperature aqueous zinc-ion battery. *Advanced Materials*, 36(26), 2403803.
- [10] Durmus, Y. E., Montiel Guerrero, S. S., Tempel, H., Hausen, F., Kungl, H. & Eichel, R.-A. (2019). Influence of Al alloying on the electrochemical behavior of zn electrodes for zn–air batteries with neutral sodium chloride electrolyte. *Frontiers in Chemistry*, 7, 800.
- [11] Lu, B., Li, Y., Wang, H., Wang, Y., Yu, W., Wang, Z. & Xu, G. (2023). Effects of cooling rates on the solidification behavior, microstructural evolution and mechanical properties of Al–Zn–Mg–Cu alloys. *Journal of Materials Research and Technology*, 22, 2532-2548.
- [12] Liu, X., Zhao, Q. & Jiang, Q. (2020). Effects of cooling rate and TiC nanoparticles on the microstructure and tensile properties of an Al–Cu cast alloy. *Materials Science and Engineering: A*, 790, 139737.
- [13] Fabris, R., Masi, G. & Bignozzi, M.C. (2024). Corrosion behavior of aluminum alloys in different alkaline environments: effect of alloying elements and anodization treatments. *Coatings*, 14(2), 240-257.
- [14] Yang, J., Yin, B., Sun, Y., Pan, H., Sun, W., Jia, B., Zhang, S. & Ma, T. (2022). Zinc anode for mild aqueous zinc-ion batteries: challenges, strategies, and perspectives. *Nanomicro Letters*, 14(1), 42.
- [15] Naveed, A., Rasheed, T., Raza, B., Chen, J., Yang, J., Yanna, N. & Wang, J. (2022). Addressing thermodynamic instability of Zn anode: classical and recent advancements. *Energy Storage Materials*. 44, 206-230.
- [16] Zeng, Y., Gaskey, B., Benn, E., McCue, I., Greenidge, G., Livi, K., Zhang, X., Jiang, J. & Elebacher, J. (2019). Electrochemical dealloying with simultaneous phase separation. *Acta Materialia*, 171, 8-17.
- [17] Neogi, A. & Janisch, R. (2022). Unravelling the lamellar size-dependent fracture behavior of fully lamellar intermetallic γ -TiAl. *Acta Materialia*, 227, 117698.

- [18] Minho, O., Tanaka, Y. & Kobayashi, E. (2023). Microstructure evolution at the interface between Cu and eutectic Sn–Bi alloy with the addition of Ag or Ni. *Journal of Materials Research and Technology*, 26, 8165-8180.
- [19] Xia, Y., Lu, Z., Han, J., Zhang, F., Wei, D., Watanabe, K. & Chen, M. (2022). Bulk diffusion regulated nanopore formation during vapor phase dealloying of a Zn-Cu alloy. *Acta Materialia*, 238, 118210.